

Lithosphere structure underneath the Tibetan Plateau inferred from elevation, gravity and geoid anomalies

Ivone Jiménez-Munt ^{a,*}, Manel Fernàndez ^a, Jaume Vergés ^a, John P. Platt ^b

^a *Group of Dynamics of the Lithosphere, Institute of Earth Sciences 'J. Almera' - CSIC, Sole Sabaris s/n, 08028 Barcelona, Spain*

^b *Department of Earth Sciences, University of Southern California, Los Angeles, CA 90089-0740, USA*

Received 30 January 2007; received in revised form 22 November 2007; accepted 23 November 2007

Available online 8 December 2007

Editor: C.P. Jaupart

Abstract

The Tibetan Plateau is the product of crustal thickening caused by collision between India and Asia. Plate tectonic reconstructions suggest continuous northward movement of the Indian plate relative to stable Eurasia at nearly 50 mm/yr for the last 50 My. The plateau is now at ~5 km elevation with steep topographic gradients across the southern and northern margins. These steep topographic gradients are also related to large lateral variations in the geoid and gravity anomalies. In a SSW to NNE cross section, the Bouguer gravity anomaly decreases over a distance of 500 km from about 0 mGal in the India plate to ~−500 mGal on the Tibetan Plateau. The geoid anomaly also presents steep gradients on both the Himalayan front and the northern margin, reaching values between 20–30 m on the plateau, suggesting a pronounced thinning of the lithospheric mantle. Uplift late in the tectonic evolution of the plateau, the widespread extension, and the associated magmatism have been attributed to convective removal of the lower part of lithospheric mantle and its replacement by hotter and lighter asthenosphere. Here we present a two-dimensional lithospheric thermal and density model along a transect from the Indian plate to Asia, crossing the Himalaya front and the Tibetan Plateau. The model is based on the assumption of local isostatic equilibrium, and is constrained by the topography, gravity and geoid anomalies and by thermal data within the crust. Our results suggest that the height of the Tibetan Plateau is compensated by thick crust in the south and by hot upper mantle to the north. The Tibetan Plateau as a whole cannot be supported isostatically only by thickened crust; a thin and hot lithosphere beneath the northern plateau is required to explain the high topography, gravity, geoid and crustal temperatures. The lithosphere reaches a maximum depth of ~260 km beneath the southern Plateau, and thins abruptly northward to ~100 km under the central and northern Plateau. The lithosphere depth increases again beneath the Qaidam basin and the Qilian Shan to ~160 km.

© 2007 Elsevier B.V. All rights reserved.

Keywords: modelling; asthenosphere; lithosphere removal; uplift; potential fields

1. Introduction

The deep structure of the India–Asia collision and the Tibetan Plateau has been a subject of debate for a long time. The Cenozoic collision between the Indian and Asian continents formed the Tibetan Plateau, beginning at about 55 Ma with an average 50 km/My N–S convergence. Since this time, at least

1400 km of convergence has been absorbed within the Himalayan–Tibetan orogen (Yin and Harrison, 2000) by a combination of several mechanisms. A wide variety of hypotheses have been proposed for Tibetan tectonic evolution, such as crustal shortening and thickening by pure shear during the Mesozoic and Cenozoic (Murphy et al., 1997) or entirely during the Cenozoic (Houseman and England, 1993), delamination or convective removal of tectonically thickened lithospheric mantle (England and Houseman, 1989; Molnar et al., 1993; Platt and England, 1994; Jiménez-Munt and Platt, 2006), block extrusion along major strike-slip faults (Tapponnier et al., 2001), and thrusting of the Indian mantle lithosphere under Asia

* Corresponding author.

E-mail addresses: ivone@ija.csic.es (I. Jiménez-Munt), mfernandez@ija.csic.es (M. Fernàndez), jverges@ija.csic.es (J. Vergés), jplatt@usc.edu (J.P. Platt).

(Owens and Zandt, 1997). Some studies have proposed combinations of more than one of these mechanisms for thickening and uplift of the plateau. The seismicity indicates that normal and strike-slip faulting occur at elevations above 4 km, with consistent east-west orientation of crustal extension (Molnar and Lyon-Caen, 1989). Thrust faulting in regions with lower elevations continues to build a thicker crust and to elevate the margins of the plateau.

The 2-D lithospheric model presented in this study traverses 2300 km along a SSW–NNE trending transect crossing, from India to Asia, the eastern region of the Himalaya, Tibetan Plateau, Qaidam Basin, Qilian Mountains and Beishan. This region has experienced a long history of accretion, arc and microcontinental collisions, and associated tectonism during the Phanerozoic, resulting in a wide variety of geological composition and structure. In the following paragraphs we review the likely crustal structure and tectonic evolution of these terranes in turn.

Peninsula India south of the Himalaya is largely composed of the Precambrian Indian shield, which is itself a collage of cratons and intervening mobile belts assembled between mid-Archean and neo-Proterozoic time (Naqvi and Rogers, 1987), and carved into a peninsula by south-tapering passive continental margins that are covered by a thin veneer of Phanerozoic sediments. The Himalayan fold and thrust belt marks the northern collisional boundary of India with Tibet, and lies between the Indian shield and the Indus–Tsangpo Suture (Fig. 1). It consists of three major tectonic slices, each of which shows extensive internal imbrication and thrusting: the Lesser Himalaya, Greater Himalaya and Northern or Tethyan Himalaya. They are all considered to have been formed from the north-facing Himalayan passive continental margin, which developed from middle Proterozoic to Cretaceous times (Yin and Harrison, 2000). The Greater Himalaya in particular shows extensive high-grade metamorphism, partial melting, and intrusion by anatectic granites. It was exhumed by normal-

sense motion along the South Tibetan detachment, which separates it from the Tethyan Himalaya. The Himalaya as a whole is separated from the Tibetan Plateau proper by the Indus–Tsangpo Suture, which marks the original boundary between the Indian and Asia continental masses.

In the eastern part of the Tibetan Plateau, which is the widest, five major crustal blocks can be distinguished: the Lhasa, Qiangtang, Songpan–Ganzi, Kunlun–Qaidam and Qilian Shan terranes (Fig. 1). Each of these represents a separate arc, accretionary complex, or microcontinental fragment that was progressively accreted to the southern Asian margin during the Phanerozoic.

The Lhasa terrane is bounded by the Indus–Tsangpo Suture and the Bangong–Nujiang Suture, and it collided with Qiangtang to the north in the late Jurassic (Dewey et al., 1988). The Lhasa terrane is about 300 km wide at longitude 91°E and narrows westwards. Sedimentary strata consist of a sequence of Ordovician and Carboniferous to Triassic shallow marine clastic sediments, and the basement is mid-Proterozoic to early Cambrian in age (Yin and Harrison, 2000). The Lhasa terrane probably rifted away from northern Gondwana during Triassic time and collided with the southern margin of the Qiangtang terrane in Late Jurassic–middle Cretaceous time (Dewey et al., 1988). Along its southern margin, the Paleozoic and Mesozoic sequences are intruded by the dominantly Cretaceous to Tertiary Gangdese batholith belt, which formed an Andean-style continental margin arc above the subducting Neotethyan oceanic slab.

The Qiangtang terrane lies between the Bangong–Nujiang and the Jinsha Sutures, and is about 500 km wide in central Tibet. It rifted off of northern Gondwana during late Paleozoic time and collided with Eurasia in late Triassic–early Jurassic time. It comprises a high-pressure/low temperature metamorphic complex of Early Triassic age lying structurally beneath Late Paleozoic to Jurassic shallow marine carbonate

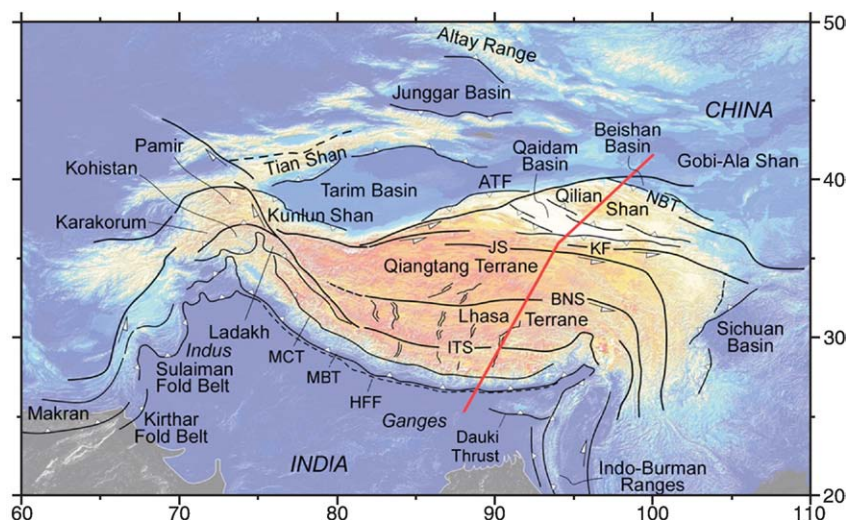


Fig. 1. Tectonic map of the Tibetan plateau and surrounding regions. Colour shades show elevation. Red line shows the position of the modelled profile. ATF: Altyn Tagh Fault, HFF: Himalayan Frontal Fault, MBT: Main Boundary Thrust of Himalaya, MCT: Main Central Thrust, ITS: Indus–Tsangpo Suture, BNS: Bangong–Nujiang Suture, JS: Jinsha Suture, KF: Kunlun Fault, NBT: North Border Thrust.

rocks interbedded with terrestrial clastic and volcanoclastic strata (Yin and Harrison, 2000).

The Songpan–Ganzi terrane is a triangular tectonic element and in the central Tibet it extends in a narrow belt about 100 km wide, between the Qiangtang terrane and the Kunlun–Qaidam terrane. It is characterized by a thick sequence of deep marine Triassic strata, commonly referred as the Songpan–Ganzi flysch complex.

Northward there is the eastern Kunlun–Qaidam terrane bounded to the north by the southern Qilian Suture. In the south, it is dominated by a broad Early Paleozoic arc, on which a younger and narrower Late Permian to Triassic arc was superposed (Yin and Harrison, 2000). The northern part is mostly occupied by the Qaidam basin.

The Qilian Shan is the northern terrane of the Tibetan Plateau, and it consists of complexly deformed early Paleozoic arcs, which were developed at the southern margin of the North China craton before it was offset by the Altyn Tagh fault in the Cenozoic (Yin and Harrison, 2000).

Recent geophysical and geological studies indicate that the Tibetan Plateau has a heterogeneous structure in the crust and lithospheric mantle (Nelson et al., 1996; Owens and Zandt, 1997; Hacker et al., 2000; Wei et al., 2001) and widespread post-collisional magmatism (Turner et al., 1993, 1996; Chung et al., 2005, and references therein). High-potassium magmas mixed with a mantle component have erupted on the Tibetan Plateau since ~45 Ma, with major pulses of activity during late Eocene–Oligocene time in the Qiangtang terrane and during the Miocene–Quaternary in the Songpan–Ganzi and Lhasa terranes (Turner et al., 1993). Widespread geothermal activity and several independent geophysical and petrological data sets indicate that the crust of the Tibetan Plateau is abnormally hot, although the debate persists whether partial melt is pervasive throughout the plateau or restricted to the extensional grabens (Nelson et al., 1996; Owens and Zandt, 1997; Alsdorf and Nelson, 1999; Hacker et al., 2000; Wei et al., 2001; Kind et al., 2002). Seismic reflection and magnetotelluric profiling in southern Tibet have revealed the presence of fluid concentration at 15 km depth (Brown et al., 1996). The shallow Curie isotherm suggested by the pronounced low satellite magnetic anomaly associated with the Tibetan Plateau (Alsdorf and Nelson, 1999), active volcanism widespread across the Qiangtang block, and magnetotelluric results (Wei et al., 2001), all support the hypothesis that melt exists within the crust of central and northern Tibet.

The structure beneath the Tibetan Plateau started to be delineated with the results of the Sino–American PASSCAL broadband experiment (Owens and Zandt, 1997; McNamara et al., 1997), the international and multidisciplinary INDEPTH experiments (Nelson et al., 1996; Zhao et al., 2001), and the series of Sino–French seismic studies (Hirn et al., 1995; Galvé et al., 2002; Jiang et al., 2006). A large diversity of geophysical methods has been used to study the lithosphere of the Himalaya and Tibet regions, such as deep seismic (Hauck et al., 1998; Galvé et al., 2002; Haines et al., 2003; Meissner et al., 2004; Jiang et al., 2006), seismic tomography (McNamara et al., 1997; Villaseñor et al., 2001), magnetotellurics (Wei et al., 2001;

Unsworth et al., 2004), gravimetry (Jin et al., 1996; Braitenberg et al., 2000), seismology (Mitra et al., 2005) and geothermics (Chung et al., 2005). These geophysical studies mostly defined the crustal structure whereas the mantle lithosphere remained little constrained. However, most of those data have been interpreted separately and the structure and geodynamics of the mantle beneath the plateau have been subject to different interpretations. This led us to the application of an integrated lithospheric modelling, based on the combined interpretation of geophysical (topography, gravity, geoid and thermal) and geological data.

In this paper we present a 2-D lithospheric thermal and density model along a SSW–NNE trending transect crossing the eastern region of the Himalaya and Tibetan Plateau from India to Asia. The model is based on the assumption of local isostatic equilibrium and constrained by the topography and by gravity and geoid anomalies. The main objective of this study is to model the lithosphere structure beneath the Tibetan Plateau and its margins, and its consequences in terms of the geodynamic evolution.

2. Method and data analysis

The numerical model used is based on the integration of regional elevation, gravity, geoid and thermal data together with available seismic data. The combined interpretation of these data provides information on the density and temperature distribution at different depth ranges. Whereas short-wavelength gravity anomalies and surface heat flow variations are sensitive to shallow structures, elevation, geoid height and long-wavelength heat flow variations are more sensitive to deep structures. Seismic data provide valuable information on both the geometry of crustal layers and the depth distribution of P-wave velocities.

Geopotential, lithostatic and heat transport equations were solved simultaneously using a finite element code based on Zeyen and Fernández (1994). The lithospheric section is divided into a number of bodies with different material properties: thermal conductivity, radiogenic heat production (which can vary with depth), and density (which can vary with pressure and temperature). The top and bottom of the model correspond to the Earth's surface and the lithosphere–asthenosphere boundary, respectively. The density of the lithospheric mantle is assumed to be temperature dependent according to $\rho_m = \rho_a(1 + \alpha \cdot (T_a - T(z)))$, where ρ_a is the density of the asthenosphere, α is the thermal expansion coefficient, and T_a is the temperature of the asthenosphere. Temperature distribution and surface heat flow are calculated by solving the steady-state heat transport equation assuming no heat flow across the lateral boundaries and fixed temperatures at the top and bottom of the model of 5 °C and 1350 °C, respectively. The Bouguer gravity anomaly is calculated using Talwani's 2D algorithm (Talwani et al., 1959) for each triangular element of the finite element mesh allowing for density variations depending on pressure, temperature, and lithology. The geoid anomaly is calculated using an algorithm based on the resolution of the gravity potential for a rectangular prism, which is formed by adjacent

triangular elements and extends to infinity in a direction perpendicular to the strike of the lithospheric section (Zeyen et al., 2005). Elevation is calculated for every column of the mesh by comparing its buoyancy with that corresponding to the average mid-oceanic ridge column under the assumption of local isostasy and following Lachenbruch and Morgan (1990). The depth of isostatic compensation to calculate elevation, and gravity and geoid anomalies is taken at the maximum depth reached by the lithospheric mantle along the transect. The space between this depth and the base of the model is filled with asthenospheric material with a constant density. The resulting elevation, Bouguer anomaly, geoid height variation, and surface heat flow or crustal temperatures are compared with the measured values. An initial crustal model is constructed by compiling available seismic data and other geophysical studies, and then the geometries of the lithosphere–asthenosphere boundary and crust are modified until the best fit is obtained. Clearly, the degree of freedom in modifying the geometry of the crustal layers depends on the availability and quality of seismic data. This modelling technique has been applied in different geodynamic settings to determine the crustal and lithospheric structure, including the Pyrenees (Zeyen and Fernández, 1994),

the High-Middle Atlas (Zeyen et al., 2005), and the Vøring and the SW Iberian margins (Fernández et al., 2004a,b).

The selected 2D lithosphere profile crosses the easternmost part of the Tibetan Plateau (line from Figs. 1 and 2), from the Indian shield (87°E, 23.46°N) to the southern Qaidam Basin (94°E, 36°N) and northeastward to the Beishan Basin (100°E, 41.5°N). It follows the major geophysical studies done in the plateau: INDEPTH I and II (Hauck et al., 1998), PASSCAL (Unsworth et al., 2004), and the Golmud–Ejn transect (Rui et al., 1999). Our main interest was the Tibetan Plateau and its margins, although we extended the profiles ~400 km south into the Indian plate and north into the Beishan Basin to avoid border effects and to model lithosphere mantle depths. Therefore, the modelling approach searches a good fit to gravity, geoid, topography and thermal data along the 2300 km long profile.

The topographic data we used is taken from GINA Global Topo Data (<http://www.gina.alaska.edu>), with values in a 30 s grid spacing (Fig. 2a). The plateau is now at an average elevation of 5 km with steep topographic gradients across the southern and northern margins. At the Himalayan front, the elevation increases from 100–300 m in the Indian plate to ~5000 m in the plateau in

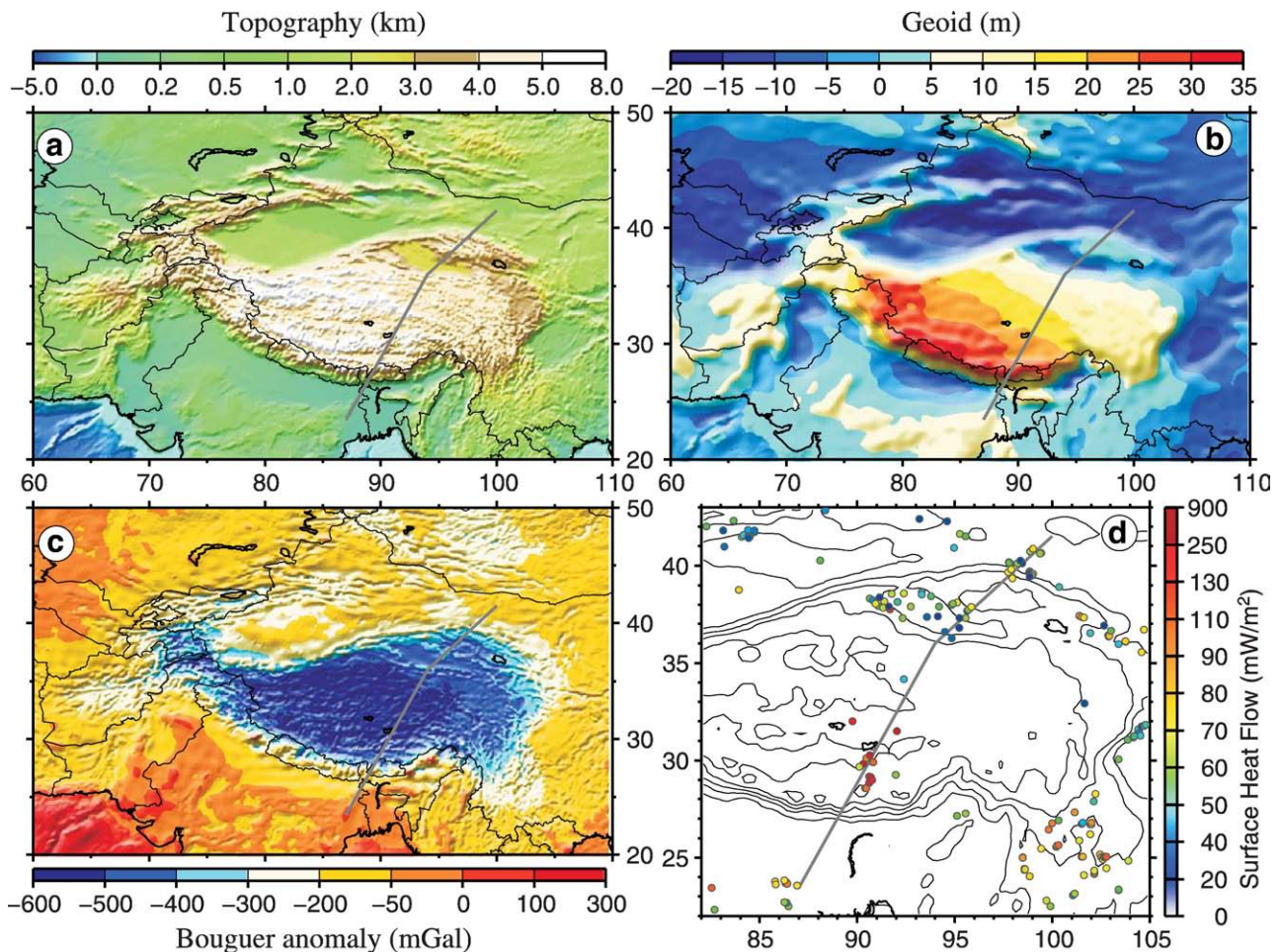


Fig. 2. Data: a) topography; b) geoid (Lemoine et al., 1998); c) Bouguer gravity calculated from global free air (Sandwell and Smith, 1997) with the 3D topographic correction (Fullea et al., submitted for publication); d) surface heat flow measurements from the global data set (Pollack et al., 1993) and from the Golmud–Ejn transect between Qaidam and Beishan basin (Rui et al., 1999). Grey line shows the position of the modelled profile. Note that d) is at a larger scale than the other figures.

less than 200 km horizontally. Also, on the northern margin, north of the Qaidam Basin (with a relative topographic minimum, 2700 m) and the Qilian Shan (~4500 m), the elevation presents a steep gradient decreasing below 1000 m.

Geoid height (Fig. 2b) is taken from the EGM96 global model (Lemoine et al., 1998). In order to avoid effects of sublithospheric density variations on the geoid, we have removed the geoid signature corresponding to the spherical harmonics developed until degree and order 8. The geoid anomaly also presents a steep gradient at the Himalayan front and the northern margin. The values over the Himalaya are between 30 and 35 m, and they smoothly decrease to 10 m towards the NE on the plateau. Farther to the NE, negative geoid anomaly values are recorded in the Qaidam Basin (−7 m) and in the Beishan region (−12 m). Negative values are also observed west to the profile coinciding with the Tarim Basin and the Himalayan front.

The Bouguer gravity anomaly (Fig. 2c) is calculated from the global free air anomaly database (Sandwell and Smith, 1997) to which a full 3D topographic correction following the methodology described by Fullea et al. (submitted for publication) has been applied using a density reduction of 2670 kg m^{-3} . The Bouguer anomaly on the Indian plate is $\sim 0 \text{ mGal}$ and it decreases to the north down to $\sim -500 \text{ mGal}$ on the Tibetan Plateau, being the lowest Bouguer anomaly values on Earth. North of the Qaidam Basin the Bouguer anomaly starts to increase reaching -150 mGal in China. Seismic studies crossing the plateau found a thick crustal root underneath the plateau, which would be in agreement with this high elevation and low values of the Bouguer gravity anomaly.

Thermal data come from several sources. The heat flow data (Fig. 2d) is taken from that compiled on the global data set (Pollack et al., 1993) and those measurements done on the Golmud–Ejn transect between Qaidam and Beishan basin (Rui et al., 1999). Heat flow measurements in the Tibetan Plateau are scarce and they include measurements on lake floors, water exploration wells and oil wells. The reported values show a high scatter probably related to active groundwater flow and magmatism as evidenced by the presence of numerous geysers, hot springs and volcanic activity. In spite of that, heat flow data suggest a decreasing trend from south to north, with values of $\sim 100 \text{ mW/m}^2$ and higher in the south and around 60 mW/m^2 in

the north. In addition to heat flow measurements, we also use indirect thermal data to constrain the temperature at different crustal and lithospheric levels. Seismic detection of the α - β quartz transition suggests a temperature of 700°C between the upper and the middle ($18 \pm 2 \text{ km}$) crust under the southern Qiangtang block and 800°C at $32 \pm 3 \text{ km}$ depth in the northern Lhasa block (Mechie et al., 2004). Hacker et al. (2000) also found temperatures between 800 – 900°C at 0.8 – 1.3 GPa (30 – 50 km) in the central Qiangtang from analyses on xenolith samples. However, Galve et al. (2006) propose lower temperatures from P-wave velocity data, and depending on composition they suggest values of $\sim 500^\circ\text{C}$ and 850°C between 1 and 2 GPa (37 and 70 km) in the lower crust under the Tethyan Himalayan.

3. Crustal structure

An initial crustal model based mainly on available seismic data was constructed to start the lithosphere modelling. The geometry of the different crustal layers was inferred from seismic profiles where available (Hauck et al., 1998; Haines et al., 2003; Mitra et al., 2005; Zhang and Klemperer, 2005; Jiang et al., 2006). Crustal and upper mantle densities have been calculated at some sites along the transect from the proposed seismic velocities (V_p and V_s) and using the velocity–density relation of Christensen and Mooney (1995).

In the Indian plate and the southern Tibetan Plateau we used the results from the deep seismic reflection profiles of the INDEPTH I and II projects (Hauck et al., 1998), and the results by Mitra et al. (2005) from teleseismic receiver function analysis. These works helped us to fix the thicknesses of the Indian foreland basin, upper and lower crust, and the geometry of the main Himalayan thrust, Lesser and Greater Himalayan units, the Tethyan Himalaya, and the Gangdese batholith (Fig. 3). From these studies we deduced a crustal thickness on the Indian plate of 40 km , which increases to 75 – 80 km beneath the northern Tethyan Himalaya and the southern Lhasa terrane.

The INDEPTH III project provides valuable information about the crustal thickness and density/depth variations in the northern Lhasa terrane from a W–E wide angle seismic profile (Zhang and Klemperer, 2005); and in the southern Qiangtang terrane from reflection data (Haines et al., 2003; Zhao et al.,

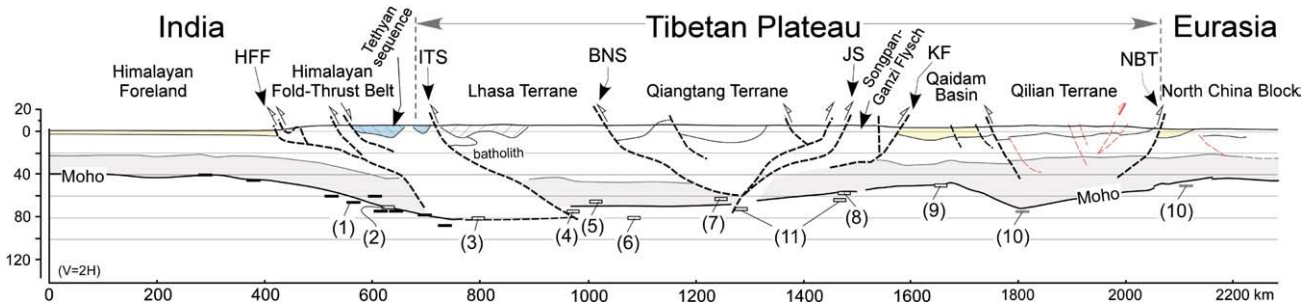


Fig. 3. Crustal structure along the profile inferred from geological (Yin and Harrison, 2000) and geophysical data. Bars show some moho depth constraints from several geophysical experiments: (1) black marks (Mitra et al., 2005), (2) (Hauck et al., 1998), (3) (Zhao et al., 2001), (4) (Owens and Zandt, 1997; Meissner et al., 2004), (5) (Haines et al., 2003), (6) (Zhang and Klemperer, 2005), (7) (Owens and Zandt, 1997; Zhao et al., 2001; Haines et al., 2003), (8) (Owens and Zandt, 1997; Zhao et al., 2001; Kind et al., 2002), (9) (Jiang et al., 2006; Zhao et al., 2006), (10) (Rui et al., 1999), (11) (Vergne et al., 2002).

Table 1
Physical parameters of the different bodies used in the modelling

<i>n</i>	Description	Lithology	<i>H</i>	<i>K</i>	ρ	<i>V</i> and [Ref.]
1	Tertiary Indian foreland basin		1.5 exp ($-z/15$)	2.3	2450	$V_s=2\text{--}2.75$ (Mitra et al., 2005)
2	India UC-lesser Himalayan	Precambrian clastic sediments and metasediments	2.2 exp ($-z/15$)	2.5	2700 2890	$V_s=3.5\text{--}3.8$ (Mitra et al., 2005)
3	Greater Himalayan belt	Late Precambrian to early Paleozoic metasedimentary rocks tectonically overlain by thick Permian to Cretaceous Tethyan sedimentary sequences. Mica schist, quartzite, paragneiss, orthogneiss, migmatite, and Miocene leucogranite.	2.5 exp ($-z/15$)	2.5	2750 2910	$V_s=3.4\text{--}3.8$ (Mitra et al., 2005) $V_p>5.7$ (Hauck et al., 1998)
4	Tethyan Himalayan sequences	Unmetamorphosed to low-grade Cambrian to Eocene shallow water shelf sediments	1.2	2.3	2650 2700	$V_s=2.5\text{--}3.2$ (Mitra et al., 2005) $V_p=5.2$ (Hauck et al., 1998)
5	Gangdese Batholith	Cretaceous-Tertiary I-type plutonic complex ranging from gabbro through diorite to granite	2.0	3.0	2750	
6	Lhasa terrane UC	Ultramafic rocks. Ordovician and Carboniferous to Triassic shallow marine clastic sediments.	2.5 exp ($-z/30$)	2.2	2700 2930	density (Haines et al., 2003) $V_p=6\text{--}6.5$ (Meissner et al., 2004) $V_p=6.1\text{--}6.5$ (Zhao et al., 2001)
7	Qiangtang Basin, sediments	Triassic-Jurassic shallow marine carbonates interbedded with terrestrial clastic and volcanoclastic strata	1.2	2.3	2500 2600	density (Haines et al., 2003) $V_p\sim 5.7$ (Meissner et al., 2004)
8	Qiangtang terrane UC	Low to high grade metamorphosed melange complexes	2.5 exp ($-z/30$)	2.5	2640 3010	density (Haines et al., 2003) $V_p\sim 5.8\text{--}7$ (Meissner et al., 2004) $V_p\sim 5.6\text{--}6.5$ (Zhao et al., 2001)
9	Songpan–Ganzi terran, Kunlun	Triassic flysch complex	2.5 exp ($-z/15$)	3.0	2600 2850	$V_p=5.4\text{--}6.2$ (Jiang et al., 2006)
10	Qaidam Basin	Ordovician shallow marine strata interbedded with andesites and volcanic tuffs	1.2	2.3	2400	$V_p=5\text{--}5.5$ (Zhao et al., 2006)
11	Qaidam–Qilian Shan UC	Complexly deformed early Paleozoic arcs. Island arcs system, Precambrian gneisses, marine sediments, volcanics and clastics.	2.0 exp ($-z/15$)	2.5	2530 2920	$V_p=6\text{--}6.3$ (Jiang et al., 2006) $V_p=5.5\text{--}6.5$ (Zhao et al., 2006) $V_p=5.5\text{--}6.3$ (Rui et al., 1999)
12	Beishan, UC		2.0 exp ($-z/15$)	2.5	2550 2880	$V_p=5.9\text{--}6.2$ (Rui et al., 1999)
13	India LC		0.2	2.1	2980	$V_s=3.9$ (Mitra et al., 2005)
14	Greater Himalayan LC		0.2	2.1	3050	$V_s=4\text{--}4.2$ (Mitra et al., 2005)
15	Lhasa–Qiantang LC	Melange complexes	0.2	2.1	3050	density (Haines et al., 2003) $V_p=6.6\text{--}7.1$ (Meissner et al., 2004) $V_p=7\text{--}7.3$ (Zhang and Klempner, 2005) $V_p=6.5\text{--}7.3$ (Zhao et al., 2001)
16	Qaidam–Qilian–Beishan LC		0.2	2.1	3000	$V_p=6.5\text{--}6.8$ (Jiang et al., 2006)
17	Lithospheric mantle		0.02	3.2	3200	$[1\text{--}3.5e-5 (T-1350\text{ }^\circ\text{C})]$

n: number of material corresponds to those from Fig. 4; *H*: radiogenic heat production [$\mu\text{W}/\text{m}^3$]; *K*: thermal conductivity [$\text{W}/(\text{K}\cdot\text{m})$]; ρ : density [kg/m^3]; *V* and Ref.: velocities [km/s] used and references. Velocities are converted to densities using Christensen and Mooney relations (1995), the non linear relation (Table 8) and the linear relation for the sediment layers (Table 7). From V_s to V_p we used the relation $V_p/V_s=1.73$. UC: upper crust, LC: lower crust.

2006) and seismic wide angle data (Zhao et al., 2001; Meissner et al., 2004). Haines et al. (2003) discuss the seismic reflection and refraction data along the profile, and also propose the density structure in two columns beneath the Lhasa and Qiangtang terranes.

The crustal structure between the Qiangtang terrane and the Qaidam Basin has been constructed principally from the wide-angle profiles along north-eastern Tibet (Vergne et al., 2002; Jiang et al., 2006) and from the magnetotelluric data recorded in the PASSCAL project (Unsworth et al., 2004). These studies suggest that the crust thins from south to north by up to 20 km (Owens and Zandt, 1997; Li et al., 2006).

On the northernmost part of the profile, which includes the Qaidam Basin, the Qilian Shan and Beishan Basin, we considered the results obtained across the Golmud–Ejn transect (Rui et al., 1999). These studies include wide-angle reflection sounding and deep seismic reflection and refraction, magneto-

telluric, as well as gravimetry, magnetics and heat flow measurements. The crust gets thicker again beneath the Qilian Shan (~ 74 km) and thins to the north down to 50 km underneath the Beishan Basin. The northern Qilian Shan reaches the higher elevation, but the crustal root is deeper beneath the southern Qilian Shan. Zhao et al. (2006), from seismic refraction and wide-angle-reflection data, also provide information about the Qaidam Basin concerning the thicknesses and compositions of the sedimentary, upper crustal and lower crustal layers.

Finally, we used the schematic geological cross section across the Himalayan–Tibetan orogen by Yin and Harrison (2000) to adjust the geometry of the different crustal bodies and their physical properties relevant to the model. Fig. 3 shows the crustal structure inferred by all these data. The crustal thickness in the Indian plate is between 38 and 40 km (Mitra et al., 2005). It increases north of the MBT, reaching the maximum thickness beneath the southern Lhasa terrane with values of 88 km

according to Mitra et al. (2005), or 70–80 km according to Zhao et al. (2001). Most studies agree that the Tibetan crust is thicker in the southern Lhasa terrane and thins to the north (Owens and Zandt, 1997; Zhao et al., 2001; Haines et al., 2003; Li et al., 2006). Values of the crustal thickness in the northern Lhasa terrane are between 74 km (Owens and Zandt, 1997) and 65 km (Haines et al., 2003), thinning northward to 60–65 km beneath the Qiangtang terrane (Owens and Zandt, 1997; Zhao et al., 2001; Haines et al., 2003; Li et al., 2006), and to 55–60 km in

the Songpan–Ganzi terrane and Qaidam Basin (Owens and Zandt, 1997; Zhao et al., 2001; Kind et al., 2002; Li et al., 2006). The Moho step at the Kunlun–Qaidam border is associated with a change in topography. The several bodies from Fig. 3 mainly correspond to the different terranes forming the plateau where we have differentiated sediments, upper and lower crust. The values of the physical properties considered for each body are listed in Table 1. Thermal conductivities and radiogenic heat production for the lithologies described from each

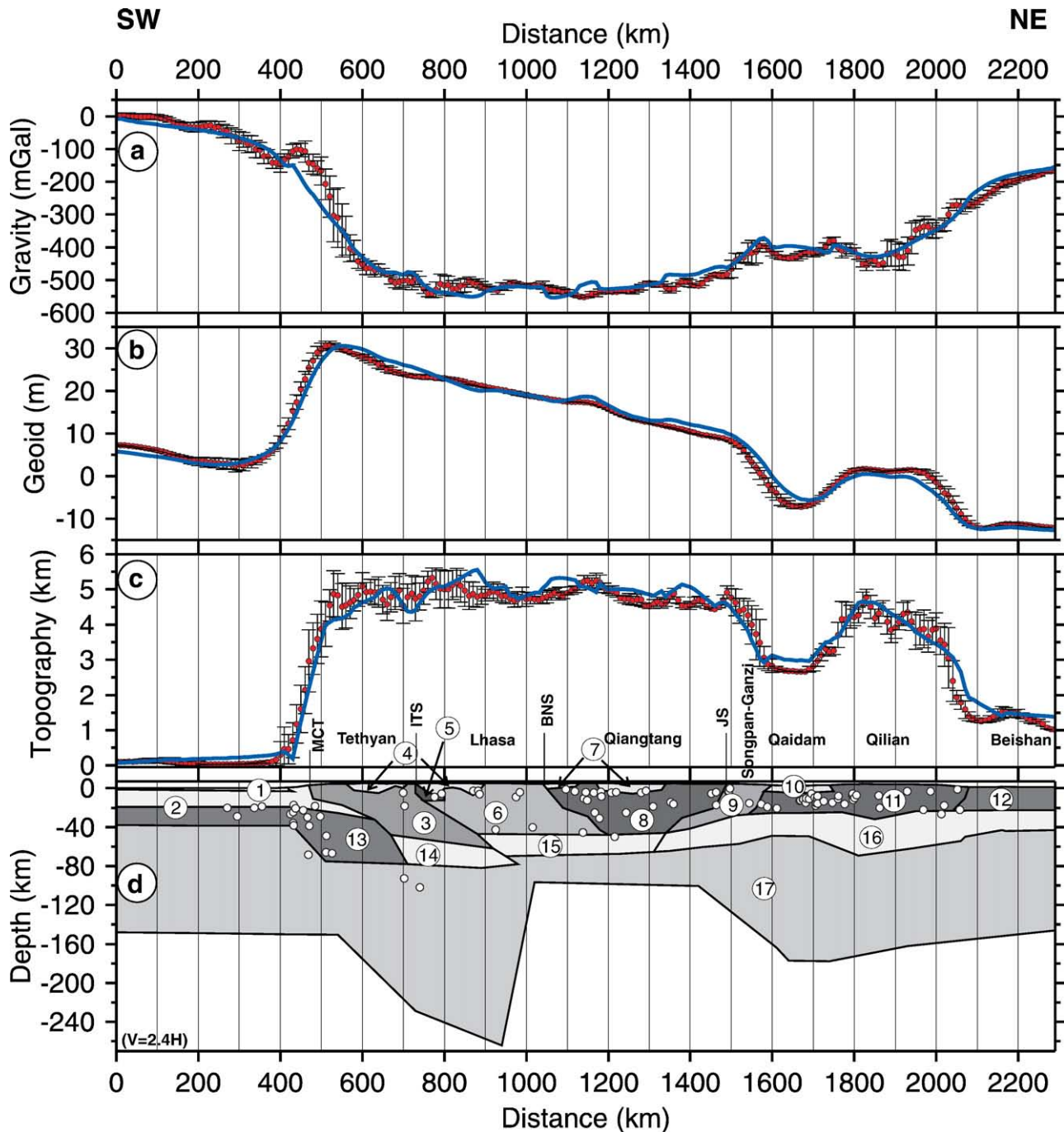


Fig. 4. Modelling results. The top three graphs (a–c) show data and results predicted from the model: a) Bouguer gravity anomaly, b) geoid and c) elevation. The data are represented by dots with bars, corresponding to the standard deviation within a range of 50 km to each side of the profile. Continuous blue lines are the modelled values. d) Lithospheric model with a vertical exaggeration of 2.4. The dots show earthquake hypocenters (Engdahl et al., 1998) projected onto the model from a strip 150 km wide each side of the model.

terrane have been taken from the literature, and densities have also been taken from literature or calculated from Vp-density relationships when possible (Christensen and Mooney, 1995).

4. Results

An initial consideration of the data, the topography and the compiled crustal structure, suggests some influence of the deep lithosphere on the isostasy of the Tibetan Plateau. The nearly uniform elevation of the plateau in spite of significant variations in crustal thickness from north to south (Fig. 3) requires corresponding variations in the upper mantle to maintain isostatic compensation. The observed thickness of the crust beneath the Himalaya and southern Tibet is enough to provide the high measured elevation; in contrast, the thinner crust in the central and northern plateau should result in a decrease of about 1400 m in elevation if a constant lithosphere thickness is considered.

The relatively abundant available data allowed us to reasonably fix the initial crustal structure and properties along the profile. Further changes in crustal thickness and densities were slight and restricted to the uncertainty range reported by the different authors and our studies. Consequently, we changed the depth of the lithosphere to fit the measured elevation, gravity and geoid.

Fig. 4 shows the observed and calculated values of Bouguer anomaly (Fig. 4a), geoid (Fig. 4b) and elevation (Fig. 4c) for the

lithosphere structure (Fig. 4d) that best fits all these observables. The data are represented by dots with dispersion bars, corresponding to the standard deviation within a range of 50 km to each side of the profile, and the continuous lines are the calculated values from the assumed model (Fig. 4d). In general, the model is in good agreement with the observables with the exception of some local misfits.

The conspicuous variations of the depth of the lithosphere–asthenosphere boundary are the most remarkable feature. The base of the lithosphere varies from 148 km beneath the Indian plate to the maximum of 264 km beneath the southern Tibetan Plateau. Northwards it thins abruptly to 98 km under the northern Lhasa and Qiantang terranes, over a region of 400 km width. The decreasing topography north of the Kunlun fault is associated with a deeper base of the lithosphere, with the maximum of 177 km underneath the northern Qaidam Basin and southern Qilian Shan. This lithosphere structure implies hotter lithospheric mantle and lower crust beneath the northern Tibetan Plateau. These results are in agreement with those inferred by several seismic studies (Haines et al., 2003; Tilmann and Ni, 2003) and review papers (DeCelles et al., 2002) where an asthenospheric upwelling is suggested underneath the northern Tibetan Plateau.

Fig. 4d also shows the earthquake hypocenters within a band 150 km on each side of the profile (Engdahl et al., 1998). Note that the deeper earthquakes occur south of the MCT, affecting

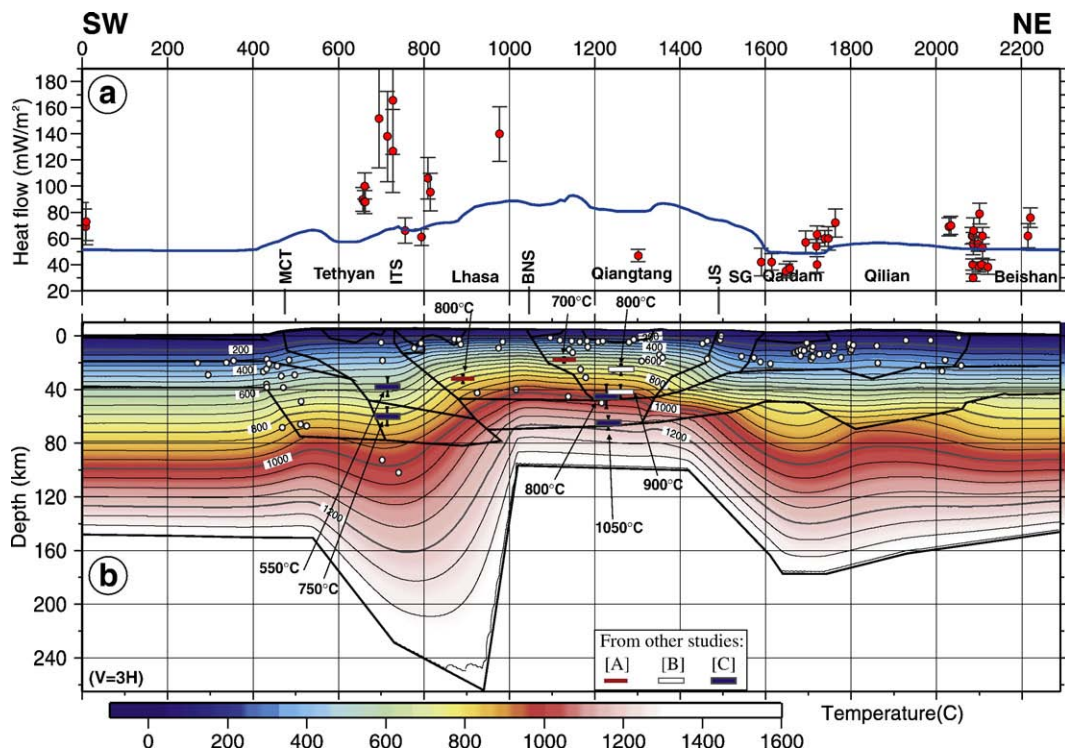


Fig. 5. a) Surface heat flow: predicted from the model (blue line) and, measurement (red dots) from Rui et al. (1999) along the profile between Qaidam and Beishan basin and global data set compiled by Pollack et al. (1993). Heat flow measurements have been projected from a 200 km half-width strip on to the profile, with the error bar dependent with the data quality ($A=0.10\%$, $B=0.15\%$, $C=0.20\%$, $D=0.25\%$); b) lithosphere temperature distribution predicted from the model (vertical exaggeration of 3). The dots show earthquake hypocenters (Engdahl et al., 1998) projected onto the model from a strip 150 km wide each side of the model. Thick horizontal bars are temperatures obtained from different studies, with the vertical lines indicating the range of values: seismic detection of the α - β quartz transition (Mechie et al., 2004, [A]), analyses on xenolith samples (Hacker et al., 2000, [B]) and, determined temperatures from P-wave velocity data and an assumed composition (Galve et al., 2006, [C]) (see Fig. 6).

the highly deformed lower crust and the uppermost mantle beneath the Greater Himalayan belt where the lithosphere is thicker and colder. Beneath the north Lhasa block and Qiangtang all the seismicity occurs within the upper and middle crust.

Fig. 5 shows the modelled surface heat flow and the lithosphere temperature distribution. The Indian plate is characterized by horizontal isotherms with moderate temperatures within the crust and the lithosphere mantle, and a Moho temperature of about 550 °C. The crustal thickening beneath the Greater Himalaya deflects the isotherms upwards near the crust-mantle boundary due to thermal refraction produced by the lower thermal conductivity of the crust relative to the lithospheric mantle. Moho temperature in this region ranges between 900 and 950 °C increasing northwards to 1150 °C. The Qiangtang region displays the maximum temperatures due to pronounced lithosphere thinning with Moho temperature ~1200 °C. Farther to the north, beneath the Qaidam, Qilian and Beishan regions, crustal temperatures decrease again showing large variations at the Moho ranging from 900 °C to less than 700 °C in Beishan. The upper panel (Fig. 5a) shows the measured surface heat flow available (Pollack et al., 1993; Rui et al., 1999) projected from a 200 km half-width strip on to the profile and the heat flow predicted by our model. Our results show large variations from ~50 mW/m² in the Indian plate and the Beishan region, to maximum values of 85–90 mW/m² in the northern Lhasa and Qiangtang regions. Despite the large scattered and uncertainties associated with the reported heat flow measurements, the general trend of measured and calculated values coincide pretty well showing low values in India, the highest in Himalaya and Lhasa block, and minima in Qaidam basin. Moreover, the calculated values at the southern and northern ends of the profile match those measured in stable lithosphere, and those in the northern Lhasa and Qiangtang regions compare well with young deformed regions elsewhere.

Fig. 6 compares the temperature and pressure/depth predicted by our model and those *P–T* conditions derived from seismic data, xenoliths and the α - β quartz transition for several lithosphere columns along the modelled transect. Galve et al. (2006) suggested temperatures from P-wave velocities beneath the Tethyan Himalayan of ~500 to 850 °C between 1 and 2 GPa. The predicted geotherm for our model in the lower crust of the Greater Himalaya is between the extremes suggested by Galve et al. (2006). However, beneath the Qiangtang and northern Lhasa block, higher temperatures compared with those from southern plateau are observed (Fig. 6) (Hacker et al., 2000; Mechie et al., 2004; Galve et al., 2006). Using a radiogenic heat production distribution in the Qiangtang and Lhasa terranes similar to that assumed for the Songpan–Ganzi and the Himalayan belt, the resulting Qiangtang temperatures at 0.8 and 1.3 GPa are ~600 and 800 °C respectively, and a bit lower beneath north Lhasa block. These values fall within the temperature range proposed by Galve et al., (2006), but they are far away from those inferred from the α - β quartz transition (700–800 °C at 0.5–0.85 GPa, Mechie et al., 2004) and from analysis of xenoliths (800–900 °C at 0.8–1.3 GPa, Hacker et al., 2000). This indicates that the pronounced lithospheric thinning affecting the Lhasa and Qiangtang regions does not

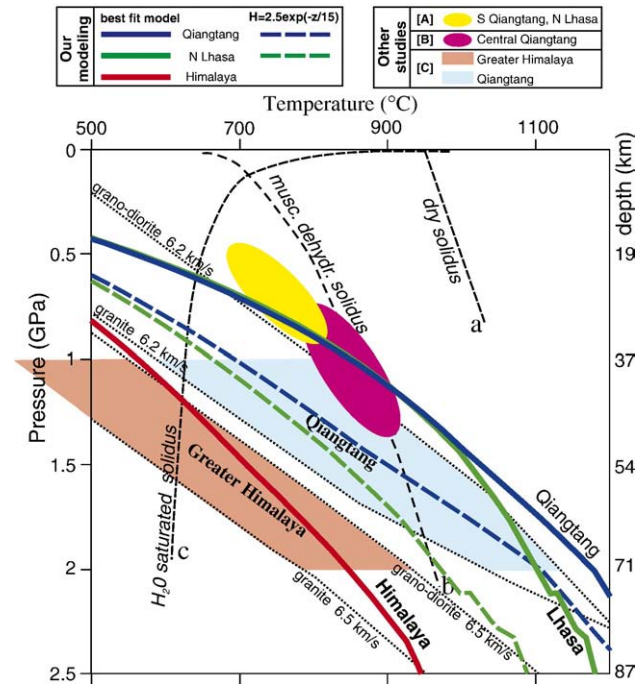


Fig. 6. Temperature in depth resulting from the model compared with some external data. Colour pattern shows the lower crustal temperatures predicted by seismic velocities (Galve et al., 2006, [C]). Yellow ellipse shows the predicted temperatures in southern Qiangtang and northern Lhasa block from the seismic detection of the α - β quartz transition (Mechie et al., 2004, [A]). Pink ellipse shows temperatures obtained by Hacker et al. (2000) [B] in central Qiangtang from xenoliths. Black dashed lines are granite solidus curves for (a) dry melting, (b) dehydration melting, and (c) wet melting. Red, green and blue lines are the resulting geotherms of our best fitting model beneath Himalaya, north Lhasa and Qiangtang terranes, respectively. Green and blue dashed lines are the geotherms of a model with lower heat production on the Lhasa and Qiangtang terranes.

suffice to explain such high temperatures at middle crustal levels. Moreover, some reflections with anomalous amplitudes (bright spots) observed at depths of 15 to 18 km on seismic lines have been interpreted as granitic magmas derived by partial melting of the tectonically thickened crust (Brown et al., 1996), thus supporting high temperatures at upper crustal levels.

In order to match these high crustal temperatures we have considered a higher characteristic length scale in the exponential radiogenic heat distribution. Therefore, we used a value of 30 km for the Qiangtang and Lhasa terranes instead of the common value of 15 km used in the upper to middle crust of the other areas (Table 1). In contrast to the other domains, the thick Tibetan crust is not formed from a cratonic terrane where the heat producing elements are mainly concentrated in the upper crust through magmatic and metamorphic processes that occurred at older times, but it has been formed by young tectonic processes that have piled up crustal slices and doubled the thickness of the crust (Dewey et al., 1988). This suggests that we should consider a smaller downward decay of the radiogenic heat production in the upper and middle crust of the Lhasa and Qiangtang terranes. This smaller decay of the radiogenic heat production on the plateau was also required by Jiménez-Munt and Platt (2006) in their modelling of the uplift

history of the plateau. Using this smaller value, Fig. 6 (solid lines) shows a good fit between the modelled geotherms beneath the Lhasa and Qiangtang terranes and those inferred from seismic, xenolith and α - β quartz transition data, although the lower crustal temperatures are just on the upper limit proposed by Galve et al. (2006). It is worth noting that the predicted V_p values (Galve et al., 2006) vary in each terrane (e.g. from 6.4 to 6.6 km/s on the Greater Himalaya) and, therefore, the P - T domains could be slightly larger than those presented on the figure. The model predicts Moho temperatures beneath the Himalaya of ~ 925 °C, whereas higher temperatures of ~ 1180 °C are obtained beneath the northern Lhasa and Qiangtang terranes.

Our transect crosses the Bayan Har domain much more further to the west than Galvé's profile (Galve et al., 2006), where this domain becomes narrowest (~ 100 km). Our calculated temperatures in the Bayan Har are lower than those from Qiangtang terrane, and higher than those proposed by Galve et al. (2006) who assumes a felsic composition (granite and granodiorite). However, Vergne et al. (2002) propose a more mafic/ultramafic rock composition according to the high V_p/V_s reported in the ~ 50 km-wide strip south of Kunlun Fault. In this case, the temperatures derived from (Galve et al., 2006) would increase noticeably and our results would fit better.

5. Discussion

The modelling approach used in this study integrates different observables: topography, Bouguer anomaly, geoid height, and temperature within the crust. These variables are governed by the density and temperature distribution within the lithosphere, which are constrained by the available geological and seismic data. The main assumptions of the model are that the lithosphere is in thermal steady state and is supported by local isostasy. These assumptions impose some limitations in interpreting the resulting lithosphere structure.

Local isostasy is an acceptable approximation, as gravity anomalies show that over length scales of a few hundreds kilometres, density contrasts within the lithosphere are isostatically compensated (England and Molnar, 1997). Furthermore, the gravity field in Tibet indicates that the topography there is for the most part in local isostatic compensation (Jin et al., 1994).

The assumption of thermal steady state is valid mostly in old lithospheres. The Himalaya and Tibetan Plateau are regions of tectonic activity that has been rapid on the time-scale for thermal equilibration of the lithosphere, and this activity is likely to have produced transient perturbations in the temperature distribution. However, quantifying these temperature variations requires a much better knowledge of the geodynamic evolution of the region. We opted for the steady-state calculations since the timing of thickness variations is too uncertain to calculate non-steady-state temperature distributions. On the other hand, this model accounts for a lithospheric density-depth distribution that is compatible with elevation, gravity, and geoid observations independent of the actual temperature distribution. The calculation in steady state minimizes the variations of lithospheric

thickness, since the modelling tends to underestimate the lithosphere thickness when thickening processes occur under transient conditions, and overestimate it for thinning processes. Therefore, the lithosphere–asthenosphere boundary beneath the Himalayan and southern Tibetan Plateau could be even deeper, whereas underneath the north Lhasa block and Qiangtang the lithosphere could be thinner. Although the numerical code also permits a temperature dependent crustal density, we have not linked the density of crustal bodies with temperature. Instead, we have derived crustal densities from measured V_p and V_s values which already incorporate compositional changes and P - T variations.

The practically constant lithospheric thickness of the Indian plate (145 km) abruptly increases north of the Main Boundary Thrust, reaching a maximum of 260 km beneath the south Lhasa block. This result agrees with the model proposed by Jin et al. (1996) where the dense mantle portion of the Indian plate has been subducted beneath the Eurasian plate for a distance of 500–700 km north of the Main Boundary Thrust. This boundary of the underthrusting Indian lithosphere is also delimited by the faster P-wave velocities in the south and slower velocities in the north of the plateau (Hearn et al., 2004).

The nearly uniform topography of the Tibetan Plateau masks the large variations in the crustal and mantle structure between the southern and northern parts. Our results show that the characteristics at depth of the northern part of the Tibetan Plateau are completely different from the south, and thinner lithospheric mantle and higher middle and lower crustal temperatures are the most remarkable features. These north-south variations are also indicated by seismic tomography data; relatively slow P_n wave velocity and inefficient S_n propagation beneath the northern half of the plateau, but relatively fast P_n wave velocity and efficient S_n propagation beneath the southern half (McNamara et al., 1997; Owens and Zandt, 1997; Tapponnier et al., 2001). Further evidences supporting a higher thermal regime in northern Tibet have long been suggested by several studies. From receiver functions, Kind et al. (2002) found that although the 410 and 660 km mantle discontinuities are parallel, both are depressed by about 20 km beneath the northern plateau relative to the south. They explain that by a northward increase in the average temperature of about 300 °C between the surface and 410 km depth. Rapine et al. (2003) find low lower-crustal S-wave velocities and the absence of an S-wave velocity gradient in the mantle beneath northern Tibet from dispersion studies, consistent with a hot and weak upper mantle. A recent global thermal model (Artemieva, 2006) also predicts higher temperatures beneath north-east Tibet than in the south. The temperatures calculated by Artemieva (2006) at 50 km depth vary from 600 °C in the south Tibet to 700 °C in the NE Tibet. At deeper levels (150 km), calculated temperatures vary from 1100 °C to 1300 °C from S to NE Tibet. The estimated lithospheric thickness, according to Artemieva (2006), varies from 180 km beneath S Tibet to 125 km beneath NE Tibet. Basaltic volcanism of different ages, but continuing until the most recent past (less than 5 Ma), is known to have occurred in northern Tibet (Yin and Harrison, 2000). Quaternary volcanism (Turner et al., 1996; Tapponnier et al., 2001) and

the unusually low P-velocities in the lower crust and upper mantle from wide-angle and refraction studies (Meissner et al., 2004), and Pn tomography (McNamara et al., 1997; Haines et al., 2003) fit perfectly into the concept of a hot, attenuated and weak lithosphere. The warm and weak layers in the lower crust and the upper mantle in the Qiangtang appear to be facilitating an easterly escape of the whole lithosphere; this eastward movement is observed by GPS data (Zhang et al., 2004) and also suggested by the strong east–west anisotropy (Meissner et al., 2004).

Haines et al. (2003) conclude from a crustal velocity model around the Bangong–Nujiang Suture (BNS) that the total pressure beneath the Lhasa and Qiangtang blocks at 65 km is the same (within 3 MPa), so that large mantle density differences to great depth below the BNS are precluded. Our results are in agreement with the lack of density variations south and north around the BNS, but large variations are predicted for the northern and southern Lhasa terrane. The good fit of topography, geoid, and gravity data to our model (Fig. 4), shows that crustal isostatic compensation of the plateau is insufficient to explain observations and requires density variations to be present in the deeper lithosphere.

Our predicted lithospheric thickness also agrees with the pattern of the elastic thickness of the lithosphere (T_e) obtained by a non-spectral technique from observed topography and Bouguer gravity anomaly data (Jordan and Watts, 2005). Considering that for temperatures higher than $\sim 800^\circ\text{C}$ the strength of the lithosphere is practically zero, we can compare the thickness of the mechanical lithosphere with the depth of this isotherm. From our modelling we find that the deepest regions of the 800°C isotherm are underneath the Himalayan foreland (~ 72 km), Qaidam Basin (~ 58 km), and in Beishan (~ 61 km). In contrast, the 800°C isotherm is at about 30 km depth beneath the northern Lhasa and Qiangtang terranes. This corresponds with the results of Jordan and Watts (2005), who found that the Himalayan foreland forms a rigid block with a thick mechanical lithosphere or equivalent elastic thickness ($T_e=40$ – 100 km),

together with the Qaidam Basin to the north and Sichuan Basin to the east; and that the Tibetan Plateau is a weaker region ($T_e=0$ – 20 km) that separates these rigid blocks. Moreover, we found that the average temperature of the lithospheric mantle beneath the Qaidam Basin is less than that of the Qilian Shan. This suggests that the Qaidam Basin has a higher lithospheric strength than the Qilian Shan, which could explain the transmission of stress through to the north of the Qaidam Basin, causing the ongoing deformation in the Qilian Shan.

5.1. Geodynamic implications

Many geodynamic models of the Tibetan Plateau invoke continuum deformation of the lithosphere, with shortening and thickening of both crust and lithospheric mantle (e.g., Houseman and England, 1993). Some of these models suggest that the thickened Tibetan lithosphere become unstable, and that the lower part was delaminated or otherwise removed, producing a localized upwelling of the asthenosphere (Molnar et al., 1993; Jiménez-Munt and Platt, 2006 and references therein). Establishing the geometry of the crustal and lithospheric structures is a key to understand the evolution of the Himalayan–Tibetan orogen.

Recent thin sheet numerical modeling indicates that rapid removal of the lithospheric root beneath the thickened crust of Tibet successfully explains the current elevation of the plateau, its lack of surface slope, the steep south and north margins, and the pattern of the present deformation (Jiménez-Munt and Platt, 2006), using the methodology describe in Jiménez-Munt et al. (2005). Two important additional results can be extracted. First, their modeling suggests that this removal took place within the last 12 My. The second result refers to the sharp boundary along the northern topographic edge of the Tibetan Plateau. This boundary can only be produced, subsequent to lithospheric thinning, by the continuous thickening of both crust and lithospheric mantle beneath the northern plateau. Thickening of the lithospheric mantle is the combined product of both

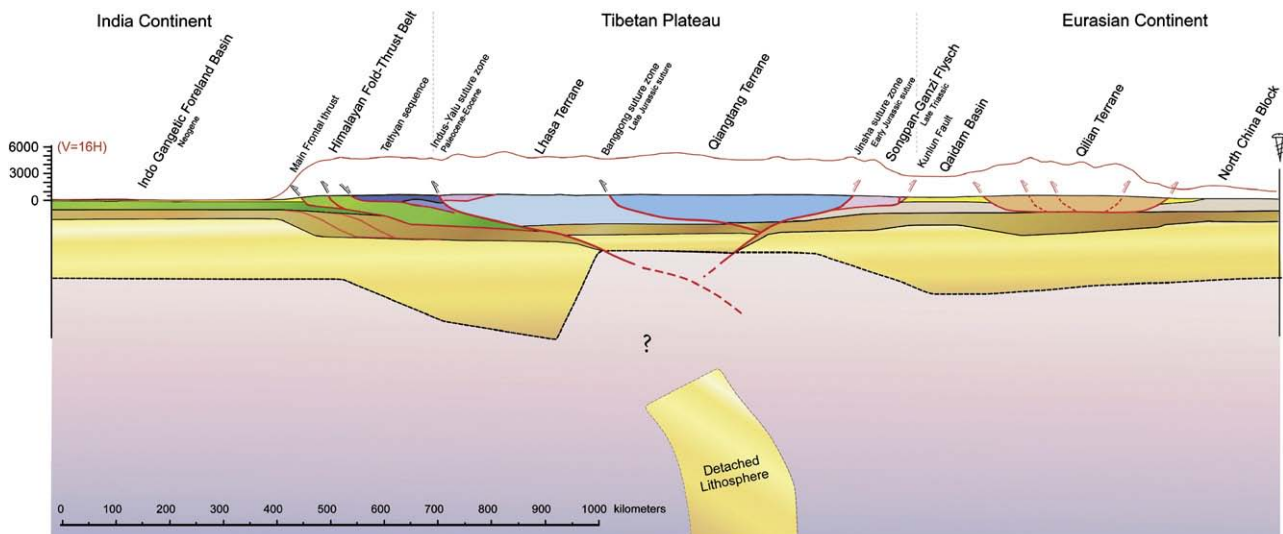


Fig. 7. Cartoon of the resulting profile, lithosphere scale.

shortening and thermal relaxation. A similar evolution can be inferred for the Tethyan Himalaya and southern Tibetan Plateau. There, continuous convergence between India and Asia has thickened the crust as well as the upper mantle, and thus modified the topography produced during lithospheric thinning at about 10 Ma.

The N–S variations of the characteristics of the lithosphere suggest some consequences for the evolution of the Tibetan Plateau. The thin and hot lithospheric mantle beneath the northern Lhasa block and Qiangtang (Figs. 4 and 5) with the onset of strong shear wave splitting anisotropy about 25 km south of the BNS, indicate that part of the thickened lithospheric mantle has been removed (Fig. 7), resulting in an upwelling of asthenospheric mantle (Molnar et al., 1993; Jiménez-Munt and Platt, 2006). Elevated temperatures and perhaps partial melting in the upper mantle would be a natural consequence of this process, and would produce the low electrical resistivities (Partzsch et al., 2000). Moreover, as mantle-derived melts migrate upward through the crust, they initiate crustal melting and pervasive low magnetic resistivity results in the lower crust (Unsworth et al., 2004). Our results are consistent with a model in which Asian lithosphere extends as far south as the Kunlun Fault and the upper mantle beneath the Songpan–Ganze and Qiangtang terranes is sufficiently hot to contain a small fraction of interconnected partial melt. The crust thins from south to north with a concomitant increase in Poisson's ratio from normal values in the south to unusually high values in the north, which also suggests that the crust of the northern plateau is partially melted due to high temperatures (Owens and Zandt, 1997). All this is also in agreement with the observed Quaternary volcanism (Turner et al., 1996; Tapponnier et al., 2001).

The lithospheric structure we obtain could therefore be in agreement with removal of the lithospheric root beneath the thickened crust of Tibet at ~8 My (Molnar et al., 1993) or within the last 12 My (Jiménez-Munt and Platt, 2006). Our model makes good sense in terms of the post-12 Ma convergence history, since convergence at 20 mm/yr for 12 My gives 240 km underthrusting, and we can be sure that Indian lithosphere extended at least as far as the Indus–Tsangpo suture before then. Moreover, our proposed lithospheric geometry is in agreement with those works that propose bidirectional underthrusting from north and south beneath Tibet. Yin and Harrison (2000) argue that the occurrence of syn-collisional calc-alkaline type volcanism in southern and central Tibet appears to require that some portion of the continental crust from both north and south must have been subducted into the mantle beneath Tibet. Rui et al. (1999) also suggest from deep seismic reflection profiles along the Northern Qilian Shan that the Ala Shan underthrusts the northern Tibetan Plateau.

6. Conclusions

Joint modelling of gravimetry, topography and geoid data, using geological and crustal seismic and thermal data as constraints, allowed us to establish a new model of the lithospheric structure of the Tibetan Plateau and its surroundings. This study allows us to image the variations of the lithosphere

thickness along a profile from the Indian plate to Beishan Basin in China, crossing the Himalayan belt and the Tibetan Plateau.

These results suggest that the coldest part of the mantle underlies southern Tibet and that the hottest underlies north central Tibet. The present average topography of the High Himalaya and Tibetan Plateau is supported by a non-uniform crustal and lithospheric structure. The High Himalaya and the southern Tibetan Plateau consist of thick crust and thick upper mantle whereas the northern Tibetan Plateau is underlain by a thinner crust and thin lithospheric mantle. The surface manifestations of such variations in mantle structure are obscured by the nearly uniform elevation of Tibet, the height of which is compensated by thick crust in the south and by hot upper mantle to the north. One of the principal conclusions is that the Tibetan Plateau as a whole cannot be supported isostatically only by a thickened crust. A thin and hot lithosphere beneath the northern plateau is required to explain the high topography, and the measured gravity and geoid.

The crust beneath southern Tibet is thicker than 70 km, and presumably some of this crust is Indian. Therefore, the Indian lithosphere appears to be being emplaced directly beneath the southern Tibetan crust. This suggests removal of Tibetan lithospheric mantle before (or during) the underthrusting of India. This corresponds well with geodynamic ideas concerning the evolution of the Indian plate (underthrusting or subduction?) and the removal of lithosphere, with the resulting upwelling of asthenosphere.

The nearly uniform elevation of the plateau above a laterally varying upper mantle is associated with corresponding variations in crustal thickness to maintain isostatic compensation. Therefore, there are different modes of isostatic support of the plateau, the southern part (Tethyan Himalaya and southern Lhasa block) by thick-low density crust and the northern part (northern Lhasa block and Qiangtang) by hot, low-density upper mantle.

We propose in this paper that lithospheric thinning was the consequence of rapid large-scale removal lithosphere at some time between 8 and 12 Ma, in agreement with geological observations as well as numerical modelling results (e.g., Molnar et al., 1993; Turner et al., 1996; Jiménez-Munt and Platt, 2006). According to the modeling by Jiménez-Munt and Platt (2006), the sudden replacement of cold mantle lithosphere by hot asthenosphere produced a rapid increase of the high Himalaya and Tibetan Plateau by about 1.5 km. The resulting plateau still sloped significantly northwards, however, reflecting the previous pattern of crustal thickening. The final increase in elevation of the northern part of the plateau, producing the present uniform elevation and the abrupt northern margin, took place about 10 My after the replacement of the upper mantle, and was the product of south to north crustal flow, continued shortening in the north, and lithospheric thermal recovery (Jiménez-Munt and Platt, 2006). Continued convergence between the Indian and Asian plates is also moving Indian lithosphere beneath the Tibetan Plateau, thickening the crust and replacing asthenospheric mantle with Indian lithosphere.

Acknowledgements

This is a contribution of the Team Consolider-Ingenio 2010 (CSD2006-00041). This research was also partly financed by Projects WESTMED (REN 2002-11230-E-MAR/01-LEC-EMA22F), SAGAS (CTM2005-08071-C03-03/MAR) and TopoAtlas (CGL2006-05493/BTE). I. Jiménez-Munt was supported by the Spanish Government by the Program ‘Ramón y Cajal’. The authors thank J. Fulla for developing the program used to calculate the Bouguer anomaly and A. Galvé for give us her figure used in Fig. 6. Constructive reviews from anonymous reviewer helped us improve the final version.

References

- Alsdorf, D., Nelson, K.D., 1999. Tibetan satellite magnetic low: evidence for widespread melt in the Tibetan crust? *Geology* 27, 943–947.
- Artemieva, I.M., 2006. Global $1^\circ \times 1^\circ$ thermal model TC1 for the continental lithosphere: implications for lithosphere secular evolution. *Tectonophysics* 416, 245–277.
- Braitenberg, C., Zadro, M., Fang, J., Wang, Y., Hsu, H.T., 2000. The gravity and isostatic Moho undulations in Qinghai–Tibet plateau. *J. Geodyn.* 30, 489–505.
- Brown, L.D., Zhao, W., Nelson, K.D., Hauck, M., Alsdorf, D., Ross, A., Cogan, M., Clark, M., Liu, X., Che, J., 1996. Bright spots, structure, and magmatism in Southern Tibet from INDEPTH seismic reflection profiling. *Science* 274, 1688–1690.
- Christensen, N.I., Mooney, W.D., 1995. Seismic velocity structure and composition of the continental crust: a global view. *J. Geophys. Res.* 100, 9761–9788.
- Chung, S.-L., Chu, M.-F., Zhang, Y., Xie, Y., Lo, C.-H., Lee, T.-Y., Lan, C.-Y., Li, X., Zhang, Q., Wang, Y., 2005. Tibetan tectonic evolution inferred from spatial and temporal variations in post-collisional magmatism. *Earth-Science Rev.* 68, 173–196.
- DeCelles, P.G., Robinson, D.M., Zandt, G., 2002. Implications of shortening in the Himalayan fold-thrust belt for uplift of the Tibetan Plateau. *Tectonics* 21, 1062. doi:10.1029/2001TC001322.
- Dewey, J.F., Shackleton, R.M., Chang, C., Sun, Y., 1988. The tectonic evolution of the Tibetan Plateau. *Phil. Trans. R. Soc. Lond. A* 327, 379–413.
- Engdahl, E.R., van der Hilst, R., Buland, R., 1998. Global teleseismic earthquake relocation with improved travel times and procedures for depth determination. *Bull. Seismol. Soc. Am.* 88, 722–743.
- England, P.C., Houseman, G.A., 1989. Extension during continental convergence, with application to the Tibetan plateau. *J. Geophys. Res.* 94, 17,561–17,579.
- England, P.C., Molnar, P., 1997. Active deformation of Asia: from kinematics to dynamics. *Science* 278, 647–650.
- Fernández, M., Marzán, I., Torne, M., 2004a. Lithospheric transition from the Variscan Iberian Massif to the Jurassic oceanic crust of the Central Atlantic. *Tectonophysics* 386, 97–115.
- Fernández, M., Torne, M., García-Castellanos, D., Vergés, J., Wheeler, W., Karpuz, R., 2004b. Deep structure of the Vøring Margin: the transition from a continental shield to a young oceanic lithosphere. *Earth Planet. Sci. Lett.* 221, 131–144.
- Fulla, J., Fernandez, M., Zeyen, H., submitted for publication. FA2BOUG- a FORTRAN 90 code to compute Bouguer gravity anomalies from gridded free air anomalies: application to the Atlantic-Mediterranean transition zone, submitted to Computers and Geosciences.
- Galve, A., Jiang, M., Hirn, A., Sapin, M., Laigle, M., de Voogd, B., Gallart, J., Qian, H., 2006. Explosion seismic P and S velocity and attenuation constraints on the lower crust of the North–Central Tibetan Plateau, and comparison with the Tethyan Himalayas: Implications on composition, mineralogy, temperature, and tectonic evolution. *Tectonophysics* 412, 141–157.
- Galvé, A., Sapin, M., Hirn, A., Diaz, J., Lepine, J.-C., Laigle, M., Gallart, J., Jiang, M., 2002. Complex images of Moho and variation of Vp/Vs across the Himalaya and South Tibet, from a joint receiver-function and wide-angle-reflection approach. *Geophys. Res. Lett.* 29, 2182. doi:10.1029/2002GL015611.
- Hacker, B.R., Gnos, E., Ratschbacher, L., Grove, M., McWilliams, M., Sobolev, S.V., Wan, J., Zhenhan, W., 2000. Hot and dry deep crustal xenoliths from Tibet. *Science* 287, 2463–2466.
- Haines, S.S., Klemperer, S.L., Brown, L., Jingru, G., Mechie, J., Meissner, R., Ross, A., Wenjin, Z., 2003. INDEPTH III seismic data: From surface observations to deep crustal processes in Tibet. *Tectonics* 22, 1001. doi:10.1029/2001TC001305.
- Hauck, M.L., Nelson, K.D., Brown, L.D., Zhao, W., Ross, A.R., 1998. Crustal structure of the Himalayan orogen at $\sim 90^\circ$ east longitude from Project INDEPTH deep reflection profiles. *Tectonics* 17, 481–500.
- Hearn, T.M., Wang, S., Ni, J.F., Xu, Z., Yu, Y., Zhang, X., 2004. Uppermost mantle velocities beneath China and surrounding regions. *J. Geophys. Res.* 109. doi:10.1029/2003JB002874.
- Hirn, A., et al., 1995. Seismic anisotropy as an indicator of mantle flow beneath the Himalayas and Tibet. *Nature* 375, 571–574.
- Houseman, G., England, P., 1993. Crustal thickening versus lateral expulsion in the Indian–Asian continental collision. *J. Geophys. Res.* 98, 12233–12249.
- Jiang, M., Galvé, A., Hirn, A., de Voogd, B., Laigle, M., Su, H.P., Diaz, J., Lepine, J.C., Wang, Y.X., 2006. Crustal thickening and variations in architecture from the Qaidam Basin to the Qang Tang (North-Central Tibetan Plateau) from wide-angle reflection seismology. *Tectonophysics* 412, 121–140.
- Jiménez-Munt, I., García-Castellanos, D., Fernandez, M., 2005. Thin-sheet modelling of lithospheric deformation and surface mass transport. *Tectonophysics* 407, 239–255.
- Jiménez-Munt, I., Platt, J.P., 2006. Influence of mantle dynamics on the topographic evolution of the Tibetan Plateau: results from numerical modelling. *Tectonics* 25, TC6002. doi:10.1029/2006TC001963.
- Jin, Y., McNutt, M.K., Zhu, Y., 1994. Evidence from gravity and topography data for folding of Tibet. *Nature* 371, 669–674.
- Jin, Y., McNutt, M.K., Zhu, Y.-S., 1996. Mapping the descent of Indian and Eurasian plates beneath the Tibetan Plateau from gravity anomalies. *J. Geophys. Res.* 101, 11275–11290.
- Jordan, T.A., Watts, A.B., 2005. Gravity anomalies, flexure and the elastic thickness structure of the India–Eurasia collisional system. *Earth Planet. Sci. Lett.* 236, 732–750.
- Kind, R., Yuan, X., Saul, J., Nelson, D., Sobolev, S.V., Mechie, J., Zhao, W., Kosarev, G., Ni, J., Achauer, U., Jiang, M., 2002. Seismic images of crust and upper mantle beneath Tibet: evidence for Eurasian plate subduction. *Science* 298, 1219–1221.
- Lachenbruch, A., Morgan, P., 1990. Continental extension, magmatism and elevation; formal relations and rules of thumb. *Tectonophysics* 174, 39–62.
- Lemoine, F.G., et al., 1998. The development of the Joint NASA GSFC and NIMA geopotential model EGM96. NASA Goddard Space Flight Center, Greenbelt, Md.
- Li, S., Mooney, W.D., Fan, J., 2006. Crustal structure of mainland China from deep seismic sounding data. *Tectonophysics* 420, 239–252.
- McNamara, D.E., Walter, W.R., Owens, T.J., Ammon, C.J., 1997. Upper mantle velocity structure beneath the Tibetan Plateau from Pn travel time tomography. *J. Geophys. Res.* 102, 493–505.
- Mechie, J., Sobolev, S.V., Ratschbacher, L., Babeyko, A.Y., Bock, G., Jones, A.G., Nelson, K.D., Solon, K.D., Brown, L.D., Zhao, W., 2004. Precise temperature estimation in the Tibetan crust from seismic detection of the α - β quartz transition. *Geology* 32, 601–604.
- Meissner, R., Tilmann, F., Haines, S., 2004. About the lithospheric structure of central Tibet, based on seismic data from the INDEPTH III profile. *Tectonophysics* 380, 1–25.
- Mitra, S., Priestley, K., Bhattacharyya, A.K., Gaur, V.K., 2005. Crustal structure and earthquake focal depths beneath northeastern India and southern Tibet. *Geophys. J. Int.* 160, 227–248.
- Molnar, P., England, P., Martinod, J., 1993. Mantle dynamics, uplift of the Tibetan Plateau and the Indian monsoon. *Rev. Geophys.* 31, 357–396.
- Molnar, P., Lyon-Caen, H., 1989. Fault plane solutions of earthquakes and active tectonics of the northern and eastern parts of the Tibetan Plateau. *Geophys. J. Int.* 99, 123–153.

- Murphy, M.A., Yin, A., Garrison, T.M., Durr, S.B., Chen, Z., et al., 1997. Significant crustal shortening in southcentral Tibet prior to the Indo–Asian collision. *Geology* 25, 719–722.
- Naqvi, S., Rogers, J., 1987. *The Precambrian Geology of India*. Oxford University Press Inc, USA.
- Nelson, K.D., Zhao, W., Brown, L.D., Kuo, J., Che, J., Liu, X., Klemperer, S.L., Makovsky, Y., Meissner, R., Mechie, J., Kind, R., Wenzel, F., Ni, J., Nabelek, J., Leshou, C., Tan, H., Wei, W., Jones, A.G., Booker, J., Unsworth, M., Kidd, W.S.F., Hauck, M., Alsdorf, D., Ross, A., Cogan, M., Wu, C., Sandvol, E., Edwards, M., 1996. Partially molten middle crust beneath southern Tibet: synthesis of project INDEPTH results. *Science* 274, 1684–1688.
- Owens, T.J., Zandt, G., 1997. Implications of crustal property variations for models of Tibetan plateau evolution. *Nature* 387, 37–43.
- Partzsch, G.M., Schilling, F.R., Arndt, J., 2000. The influence of partial melting on the electrical behavior of crustal rocks: laboratory examinations, model calculations and geological interpretations. *Tectonophysics* 317, 189–203.
- Platt, J.P., England, P., 1994. Convective removal of lithosphere beneath mountain belts: thermal and mechanical consequences. *Am. J. Sci.* 294, 307–336.
- Pollack, H.N., Hurter, S.J., Johnson, J.R., 1993. Heat flow from the Earth's interior: analysis of the global data set. *Rev. Geophys.* 31, 267–280.
- Rapine, R., Tilmann, F., West, M., Ni, J., Rodgers, A., 2003. Crustal structure of northern and southern Tibet from surface wave dispersion analysis. *J. Geophys. Res.* 108. doi:10.1029/2001JB000445.
- Rui, G., Xiangzhou, C., Gongjian, W., 1999. Lithospheric structure and geodynamic model of the Golmud–Ejin transect in northern Tibet. *Geol. Soc. Am.* 328, 9–17.
- Sandwell, D.T., Smith, W.H.F., 1997. Marine gravity from Geosat and ERS 1 satellite altimetry. *J. Geophys. Res.* 102, 10,039–10,054.
- Talwani, M., Worzel, J.L., Landisman, M., 1959. Rapid gravity computations for two-dimensional bodies with application to the Mendocino submarine fracture zone. *J. Geophys. Res.* 64, 49–59.
- Tapponnier, P., Zhiqin, X., Roger, F., Meyer, B., Arnaud, N., Wittlinger, G., Jingsui, Y., 2001. Oblique stepwise rise and growth of the Tibetan Plateau. *Science*, 294, 1671–1677.
- Tilmann, F., Ni, J., 2003. INDEPTH III seismic team, seismic imaging of the downwelling Indian lithosphere beneath central Tibet. *Science* 300, 1424–1427.
- Turner, S., Arnaud, N., Liu, J., Rogers, N., Hawkesworth, C., Harris, N., Kelley, S., van Calsteren, P., Deng, W.M., 1996. Postcollisional, shoshonitic volcanism on the Tibetan plateau: implications for convective thinning of the lithosphere and the source of ocean island basalts. *J. Petrol.* 37, 45–71.
- Turner, S., Hawkesworth, C.J., Liu, L., Rogers, N., Kelley, S., van Calsteren, P., 1993. Timing of Tibetan uplift constrained by analysis of volcanic rocks. *Nature* 364, 50–53.
- Unsworth, M., Wei, W., Jones, A.G., Li, S., Bedrosian, P., Booker, J., Jin, S., Deng, M., Tan, H., 2004. Crustal and upper mantle structure of northern Tibet imaged with magnetotelluric data. *J. Geophys. Res.* 109, B02403. doi:10.1029/2002JB002305.
- Vergne, J., Wittlinger, G., Farra, V., Su, H., 2002. Evidence for upper crustal anisotropy in the Songpan–Ganze (northeastern Tibet) terrane. *Earth Planet. Sci.* 203, 25–33.
- Villaseñor, A., Ritzwoller, M.H., Levshin, A.L., Barmin, M.P., Engdahl, E.R., Spakman, W., Trampert, J., 2001. Shear velocity structure of central Eurasia from inversion of surface wave velocities. *Phys. Earth Planet. Inter.* 123, 169–184.
- Wei, W., Unsworth, M., Jones, A., Booker, J., Tan, H., Nelson, D., Chen, L., Li, S., Solon, K., Bedrosian, P., Jin, S., Deng, M., Ledo, J., Kay, D., Roberts, B., 2001. Detection of widespread fluids in the Tibetan crust by magnetotelluric studies. *Science* 292, 716–718.
- Yin, A., Harrison, T.M., 2000. Geologic evolution of the Himalayan–Tibetan orogen. *Annu. Rev. Earth Planet. Sci.* 28, 211–280.
- Zeyen, H., Fernández, M., 1994. Integrated lithospheric modeling combining thermal, gravity, and local isostasy analysis: application to the NE Spanish Geotranssect. *J. Geophys. Res.* 99, 18089–18102.
- Zeyen, H., Ayarza, P., Fernández, M., Rimi, A., 2005. Lithospheric structure under the western African–European plate boundary: a transect across the Atlas Mountains and the Gulf of Cadiz. *Tectonics* 24, TC2001. doi:10.1029/2004TC001639.
- Zhang, Z., Klemperer, S.L., 2005. West-east variation in crustal thickness in northern Lhasa block, central Tibet, from deep seismic sounding data. *J. Geophys. Res.* 110, B09403. doi:10.1029/2004JB003139.
- Zhang, P.-Z., Shen, Z., Wang, M., Gan, W., Bürgmann, R., Molnar, P., Wang, Q., Niu, Z., Sun, J., Wu, J., Hanrong, S., Xinzhaio, Y., 2004. Continuous deformation of the Tibetan Plateau from global positioning system data. *Geol. Soc. Am.* 32, 809–812. doi:10.1130/G20554.1.
- Zhao, J., Mooney, W.D., Zhang, X., Li, Z., Jin, Z., Okaya, N., 2006. Crustal structure across the Altyn Tagh Range at the northern margin of the Tibetan plateau and tectonic implications. *Earth Planet. Sci. Lett.* 241, 804–814.
- Zhao, W., Mechie, J., Brown, L.D., Guo, J., Haines, S., Hearn, T., Klemperer, S.L., Ma, Y.S., Meissner, R., Nelson, K.D., Ni, J.F., Pananont, P., Rapine, R., Ross, A., Saul, J., 2001. Crustal structure of central Tibet as derived from project INDEPTH wide-angle seismic data. *Geophys. J. Int.* 145, 486–498.